Emergent Materials (2023) 6:147–158
https://doi.org/10.1007/s42247-022-00443-2

ORIGINAL ARTICLE

ZnO recovered from spent alkaline batteries as antimicrobial additive for waterborne paints

Guillermo P. Lopez[1] · María V. Gallegos[2] · Miguel A. Peluso[2] · Laura C. Damonte[3] · Jorge E. Sambeth[2] · Natalia Bellotti[1]

Received: 31 July 2022 / Accepted: 26 December 2022 / Published online: 30 December 2022

Abstract
Biocides are employed to prevent biodeterioration in waterborne paints. In the present study, we used zinc oxide nanoparticles (obtained from spent alkaline batteries) as biocide for indoor waterborne paint at 1.5% of the total solid content in paint. Two different zinc oxides synthesized from spent alkaline batteries, which showed photocatalyst activity, were employed as an antimicrobial agents. After leaching the anode of alkaline batteries, zinc was precipitated from the leachate liquor by introducing oxalic acid (O-ZnO) or sodium carbonate (C-ZnO).
The antimicrobial properties of the prepared oxides were tested against *Staphylococcus aureus* (bacteria), *Chaetomium globosum*, and *Aspergillus fumigatus* (fungi) using agar well diffusion method. C-ZnO inhibited the growth of all the strains studied and presented enhanced activity than O-ZnO. The better performance as antimicrobial agent of C-ZnO compared to O-ZnO was attributed to its lower crystallite size, higher amount of oxygen monovacancies, and to its lower band gap energy. The oxide with the best performance in antimicrobial activity, C-ZnO, was employed for the formulation of waterborne acrylic paints. It was observed that 1.5% C-ZnO improved the antifungal properties and antibacterial properties compared to the control sample.

Keywords Oxide semiconductors · Antimicrobial paint · Positron annihilation · Structural properties · Battery waste · Functionalized coatings

1 Introduction

In recent years, zinc oxide (ZnO) has become a critical technological material due to its structural and electrical properties [1–4]. Several publications point out that the properties of ZnO nanoparticles (NP) strongly depend on the synthesis process that affects their surface, structural, morphological, and size characteristics [5–8].

Moreover, ZnO nanoparticles have a wide range of antibacterial and antifungal activities [9–11]. Different mechanisms responsible for the antimicrobial activity of this material have been reported in the literature [12–16].

On the other hand, alkaline batteries are described as non-rechargeable batteries (primary cells), designed to be fully discharged only once and then discarded [17]. One possible effect of depleted alkaline batteries is the corrosion of their casings, which can be affected internally by their components and externally by climatic action or by the decomposition process of urban solid waste (MSW) in case they end up in a landfill. These metals leach through soils and flow through surface water courses and aquifers, polluting the environment in general [18].

Another environmental concern is biofilms formed on indoor surfaces, which are associated with health problems and have been aggravated during the pandemic [19, 20]. Certain materials used in construction, such as wood, bricks, and concrete, allow the formation of biofilms [21]. Microorganisms naturally modify the materials in which they actively grow, which is known as biodeterioration due to the impact of extracellular products they produce and, in the

✉ María V. Gallegos
mvgallegos@quimica.unlp.edu.ar

1 Centro de Investigación Y Desarrollo en Tecnología de Pinturas - CIDEPINT (CIC-CONICET-UNLP), La Plata, Argentina

2 Centro de Investigación Y Desarrollo en Ciencias Aplicadas, CIC-CONICET-UNLP, La Plata, Argentina

3 Instituto de Física, Dto. De Física, Facultad de Cs. Exactas, CCT-CONICET-UNLP, La Plata, Argentina

case of molds, their invasive growth [20]. Some examples of pathogens causing various pathologies via biodeterioration are Aspergillus fumigatus [22], Staphylococcus aureus, Clostridium difficile, Enterococcus, and Acinetobacter [23]. In this sense, the World Health Organization has expressed their concern indicating that microbiological growth must be eliminated or minimized in indoor environments [24]. Thus, the preservation of indoor hygiene is an important goal to pursue and antimicrobial paints can be considered the most promising product for the cost–benefit binomial [25]. Nano-sized ZnO is a good alternative for the formulation of bioactive paints due to its antimicrobial potential [26].

In a previous work of Gallegos et al. [27], it was reported that zinc oxides obtained from spent alkaline batteries showed a good photocatalytic performance in methylene blue (MB) degradation reactions.

The main aim of this work is to evaluate the antifungal and antibacterial activity of zinc oxides obtained from spent alkaline batteries. Then, the use of the resulting most active ZnO as an additive in functionalized coatings to prevent microbial growth and biodeterioration in buildings was then tested. To the best of the authors' knowledge, this is the first study of a functional paint formulation using ZnO recovered from spent alkaline batteries as a biocide. The fundamental purpose of this work is to introduce a way to valorize hazardous waste for the environment, as well as improve both human health and the environment. After all, this study contributes to a sustainable economy and aims to reduce environmental costs by reducing pollution.

2 Materials and methods

2.1 Zinc oxide: preparation and characterization

Zinc oxides were obtained by recycling spent batteries through a biohydrometallurgical process, as previously described by Gallegos et al. [28, 29]. First, the anode of depleted alkaline batteries was lixiviated with bio-generated sulfuric acid. In the second step, Zn^{2+} ions were precipitated from the leachate solution by the addition of two different reagents (oxalic acid, $H_2C_2O_4$, or sodium carbonate Na_2CO_3).

The obtained suspensions were kept in agitation for 1 h at 30 °C and the products were filtered, washed, and dried at 120 °C for 24 h. Lastly, the obtained solids were calcined in air at 500 °C for 2 h. The materials were designated O-ZnO (from oxalic acid) and C-ZnO (from sodium carbonate).

The nature of the particles obtained by precipitation from homogeneous solutions depends on many factors (the concentration of the reagents, reaction temperature, pH of the solution, type of anion, mixing method, etc.). It has been shown that slight variations in the above variables can lead to particles with different chemical compositions and shapes [6–8]. Also, the presence of different counterions (NO_3^-; Cl^-; SO_4^{2-}, etc.) results in different morphologies. To our knowledge, there are few or no works analyzing the effect of different precipitate agents on the final morphology, so we choose Na_2CO_3 y $H_2C_2O_4$ due to their similar chemical natures and different final reaction products (CO and CO_2).

The crystalline structure of the studied samples was characterized through X-ray diffraction (XRD) by using a Philips diffractometer using Cu Kα ($\lambda = 1.5406$ Å). Surface area values of the synthesized samples were obtained by BET method using Micromeritics Accusorb 2100 D sorptometer. The DRS–UV–vis spectra were recorded on a Perkin Elmer Lambda 35 UV–vis spectrophotometer with integrating sphere attachment and spectralon reflectance standard. The structural defects in the prepared ZnO samples were analyzed by positron annihilation lifetime spectroscopy (PALS), which allows the evaluation of vacancy defects in semiconductors.

2.2 Antimicrobial activity

The antifungal activity of the oxides was evaluated towards *C. globosum* (KU936228) and *A. fumigatus* (KU936230) strains, whereas antibacterial activity was assessed towards *S. aureus* (ATCC 6538) strains respectively. The fungal strains were isolated as in previous research works from biodeteriorated coatings [30, 31].

Firstly, the antifungal and antibacterial activity of the samples were investigated using the agar-well diffusion method, a variant of the Kirby-Bauer agar diffusion method [32, 33]. Malt extract (MEA) and Luria Bertani (LB) were used as culture mediums for the fungal and bacterial strains, respectively. The fungal inoculum was prepared with physiological solution (PS) supplemented with tween 20 (5 ppm) and the concentration was adjusted to 10^5 spores/mL by a Neubauer chamber. A total of 200 µL of the spore suspension was mixed with 15 mL of the culture medium in each plate.

After 24 h from a liquid culture which turbidity was adjusted to 0.5 of the McFarland scale, the bacterial inoculum was obtained diluting to a suspension of 10^6 CFU/mL. The bacterial suspension was scattered uniformly on the individual plates by swabbing. Three wells of 7 mm diameter (D) each, were filled with 20 mg of the corresponding oxide sample (C-ZnO and O-ZnO). Two Petri dishes were prepared as it was described above for each sample.

The plates were incubated at 28 °C for 48 h in the case of the fungi and at 30 °C for 24 h for *S. aureus*, after that, inhibition zone diameters (D) were measured. Samples with $D < 7$ mm and $D = 7$ mm (to bacterial strain) are considered showed no activity and those with $D > 7$ mm, were active.

To assess the bioactivity performance of the selected oxides from a diffusion test and considering their application in the formulation of paints, a macrodilution test was carried out in a solid medium [32, 34]. Petri dishes containing the selected oxide with different concentrations (0, 1, 2, 3, 5, 10, and 15 mg/mL) and MEA were inoculated in the center with 20 µL of the spore suspension. The test was performed in triplicate considering the reported information for the chosen concentrations [30]. The fungal strains were the same that those used in the agar diffusion assay.

The plates were incubated at 30 °C for 7 days; afterwards growth diameters were measured evaluating the relative growth inhibition by percentage (% I). The minimum inhibitory concentration (MIC), defined as those in which no growth has been recorded, was determined.

2.3 Formulation, preparation, and characterization of the functional paints

The ZnO samples with the higher antimicrobial potentialities were selected to integrate a waterborne acrylic paint indoor formulation. The composition used for the paint preparation was based on a conventional formulation for indoor acrylic paint (% by weight): distilled water (DW) 48.0%, $CaCO_3$ 28.8%, TiO_2 13.0%, acrylic resin 6.0%, and additives 4.1% [25]. The selected components (pigments, additives, and resin) were obtained commercially. The used additives were antifoam, cellulosic thickener, pH regulator, dispersant, and coalescer. The paints were prepared in a high-speed disperser located in the CIDEPINT pilot plant. Based on the formulation presented, a control paint (CP) was made without any biocide, while the experimental paints were obtained by replacing part of the $CaCO_3$ of the formulation by the selected ZnO samples (1.5 g per 100 g of total paint).

The color and gloss of the paints were measured using the CIElab color parameters using ByK-Gardner gloss-meter equipment following Ref. [35]. The color change (ΔE), was calculated as

$$\Delta E = \sqrt{(L - L_{EP})^2 + (a - a_{EP})^2 + (b - b_{EP})^2} \quad (1)$$

being L, a, and b the CIElab parameters for the control paint and L_{EP}, a_{EP}, and b_{EP}, the corresponding ones for the experimental paints (EP) with ZnO. When ΔE is above 1.5, color change is considered evident and at even higher values ($\Delta E > 6$), it becomes large [35].

The water absorption (in wt%) was determined following a procedure based on the ASTM D570 standard. This methodology relies on the determination of the difference in weight between dry paint samples and those exposed to the action of water for 7 days at 23 °C. Water permeability was determined by the funnel method. The paint was applied on a porous unglazed tile, after the drying and curing time, two glass funnels per sample were glued with inert sealant; being the area and diameter of the funnel and the stem 20 cm^2 and 3 mm, respectively. Distilled water was introduced into the funnels to fill the available capacity (flush) under laboratory conditions. Then, they were weighed at different times: 0, 24, 48, and 72 h, and by weight difference, the permeability of the film to water was determined. Loss by evaporation was estimated with control on glass. The viscosity was determined following the guidelines of the ASTM D562 standard using a Stormer viscometer. The degree of dispersion of the liquid paint samples was obtained using a grindometer, the specific weight and hiding power were also determined according to the IRAM 1109 Standard.

2.4 Fungal resistance assay

The paints were evaluated for their resistance to fungal growth through a plate test following a methodology based on the ASTM D 5590 standard [34]. The paints were applied to glass slides which were then dried under laboratory conditions and decontaminated using a UV-germicidal lamp (Philips, 20 W). The samples were placed in plates with minimal mineral medium and were inoculated with 50 µL of spore suspension (10^5 spores / mL) of the same strains used in the previous tests. In total 6 samples of each paint were tested. The plates were incubated for 1 month at 30 °C. At the end of the test, the samples were evaluated by direct observation and by using a stereoscopic microscope. To quantify the performance of the paints, a scale from 0 to 4 was used, referring to different degrees of growth (none, trace, light, moderate, and heavy, respectively) according to the covered area based on the ASTM D 5590 standard. Due to the high vacuum, previously gold-coated samples were observed by SEM using a Philips 505 brand equipment.

2.5 Bacterial biofilm resistance assay

To assess bacterial biofilm resistance of the formulated paints a procedure in inoculated liquid culture medium was followed [36]. First, 1 cm^2 glasses were painted with each of the studied paints and allowed to cure under laboratory conditions. The glass surfaces were sterilized under a UV-germicidal lamp for 0.5 h on both sides. Subsequently, the biofilm resistance assay was carried out in a liquid medium. The inoculum of *S. aureus* was obtained and mixed with LB until a concentration of 10^6 CFU/mL. Then, the painted glasses were placed in a multiwell plate and covered with inoculated LB medium. The multiwell plates containing the samples were incubated with shaking at 125 rpm at 30 °C for 7 days, after the first 48 h, the medium was periodically replaced by the fresh sterile medium. Once the biofilm formation experiment was completed, the samples were washed 3 times with phosphate-buffered saline (PBS): 0.4 g of NaCl,

0.07 g of KH_2PO_4, and 0.45 g of K_2HPO_4 in 100 mL of DW. Next, the samples were immersed in a 2.5% glutaraldehyde solution in PBS for 24 h to fix the biofilm. Then, they were dehydrated in a gradient of solutions of ethanol in water (20, 50, 70, 90, and 100% v/v) for 30 min in each solution. After dehydration, the samples were allowed to dry at room temperature, coated with gold, and observed by SEM under high vacuum conditions.

3 Results and discussion

3.1 Antimicrobial activity of ZnO nanoparticles

The antifungal activity of the ZnO obtained from spent alkaline batteries was evaluated towards *C. globosum* and *A. fumigatus* using the agar well diffusion method. The antibacterial activity of the oxides was investigated against Gram-positive *S. aureus* bacteria, by the agar-diffusion test.

Figure 1 shows the Petri dishes of the agar test with both prepared zinc oxides (O-ZnO and C-ZnO) and control dishes, with the three strains studied. The average diameters (D) of the inhibition zones are listed in Table 1. The presence of a clear zone of inhibition (nm) around the oxides is indicative of the antimicrobial activity synthesized nanomaterials possessed.

S. aureus was the most strongly inhibited strain by the two oxides. C-ZnO showed higher inhibition zones in comparison to O-ZnO (C-ZnO–28.6; O- ZnO–22.3). Even though ZnO nanoparticles displayed good antibacterial properties on both gram-positive and gram-negative bacteria, some researchers found gram-positive strains to be more resistant [37, 38]. This has been attributed to differences in external cell structures. In the case of gram-positives, they have a thick peptidoglycan layer that contains teichoic and lipoteichoic acids. In contrast, the gram-negative has a thin layer and an external cell membrane. Here, both C-ZnO and O-ZnO showed a good performance against *S. aureus*, which was the more susceptible for this test.

Concerning the fungal strains studied, greater resistance to the action of the biocide used was observed. These results are consistent with the structural characteristics of fungi, since their cell wall is much thicker than that of bacteria. In most fungal species, the inner cell wall consists of a core of β-(1,3)-branched glucan covalently linked with ~ 4% intercede and chitin [39]. C-ZnO showed a larger range of

Table 1 The antimicrobial activity of zinc oxides against *C. globosum*, *A. fumigatus*, and *S. aureus*

Strains	Zone of inhibition (mm)		
	Control	C-ZnO	O-ZnO
C. globosum	< 7	15.6 ± 1.4	< 7
A. fumigatus	< 7	18.4 ± 2.8	11.0 ± 1.0
S. aureus	= 7	28.6 ± 1.4	22.3 ± 1.3

D < 7 and D = 7 mean: (without activity) microbial growth over the sample and no zone of inhibition, respectively.

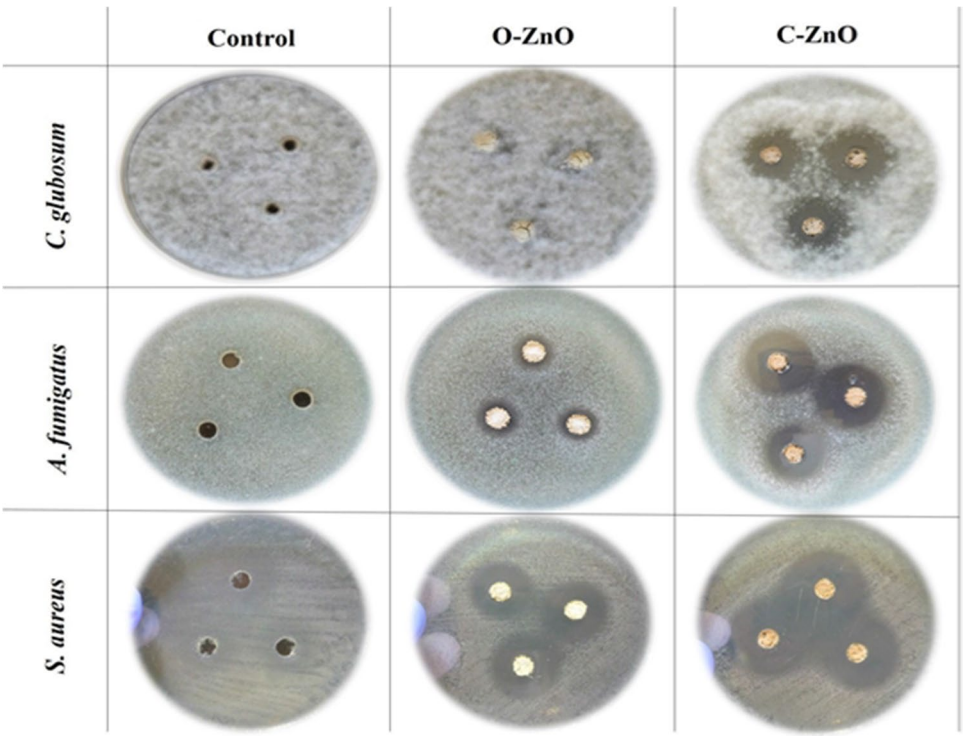

Fig. 1 Diffusion agar assay: O-ZnO, C-ZnO, and without ZnO against *C. globosum*, *A. fumigatus*, and *S. aureus*

activity than O-ZnO since it was active against both fungal strains evaluated [*C. globosum* (C-ZnO–15.6; O- ZnO—< 7) and *A. fumigatus* (C-ZnO–18.4; O- ZnO–11.0)]. It is worth mentioning that the control sample (with DW) showed no inhibition zones for any microbial studies.

In addition to the structural characteristics of the microorganisms, the bioactivity is highly dependent on ZnO NP physicochemical properties such as size, morphology, and surface defects [37, 40].

In bacteria, the bacterial cell wall is the structural layer that houses the cell membrane and cytoplasm, providing protection and structural support [41]. It is formed by peptidoglycan and its thickness determines the type of bacteria, being nanometric in size. In this regard, for a better bacteria-ZnO interaction it is necessary that the particles have nanometer dimensions [42, 43]. On the other hand, several authors have pointed out a relationship between antimicrobial activity and the morphological characteristics of the particles. Larger surface areas may provide additional antibacterial activity. With respect to the nature and concentration of defects, these contribute to the antibacterial activity of ZnO. According to Prasanna and Vijayaraghavan [44], a higher concentration of VO + + causes an increase in the generation of ROS which in turn enhances its antibacterial activity.

The above-mentioned properties are involved in the mechanisms of activity that rely on more than one cell target and it is based on: reactive oxygen species (ROS) production, the release of Zn^{2+} ions, and electrostatic interaction [45]. Studies carried out with bacteria have shown that ROS such as •OH, $\bullet O_2^-$, and H_2O_2 are significantly produced from an aqueous suspension of ZnO NP and are mainly responsible for the antibacterial activity even in the dark [37]. In this regard, it was found that surface defects in the ZnO NP play a major role in producing ROS both in the presence and absence of light. Oxidative stress in the bacterial cell can be induced by ROS which leads to the inhibition of protein synthesis and DNA replication [46], In addition, Zn^{2+} ions act as electrophiles inhibiting the glycolytic enzyme through the thiol oxidation group [47]. On the other hand, electrostatic interactions occur due to the positively charged ZnO NP which is attracted to the cell surface and is generally negatively charged; the difference in electrostatic gradient leads to cell surface damage [48].

Mosquera-Sánchez et al. found that ZnO NP showed a high inhibition of *Colletotrichum* sp. growth causing loss in the continuity of some hyphae and favoring the formation of vacuole-like structures leading to a decrease in the cytoplasmic space [49]. Kalia et al. showed the degrading effect of ZnO NP on the DNA of three filamentous fungal strains (*Macrophomina phaseolina*, *Curvularia lunata*, and *Fusarium oxysporum)* and noted that differences in size and surface functionalization diminish the antimycotic potential [50]. The effect on other kinds of organisms can be found too, for example, Shnawa et al. recently investigated the protoscolicidal activity of biosynthesized ZnO NPs with promising results reaching 100% of mortality of the protoscoleces with a concentration of 400 ppm [51]. Recently, Da silva et al. assessed the inactivation of the infectious SARS-CoV-2 on cotton fabrics with ZnO NP among other NP, reaching a reduction equal to 31% during the first 15 min [52].

The physicochemical properties of the as-prepared ZnO have been reported previously [27]. It is worthwhile to present a summary of them and their relationship with their antimicrobial activity.

Both prepared samples have the ZnO wurtzite structure. C-ZnO presents lower values of lattice cell parameters and E_{gap} (band gap energy) than O-ZnO, possibly due to a higher concentration of oxygen vacancies. Concerning the morphology of the particles, both solids presented platelet-shaped particles as can be seen by SEM images shown in Fig. 2. This fact has been reported by several authors, which indicates that the formation of this type of structure is governed by the presence of SO_4^{2-} ions adsorbed on the polar growth face. Particle sizes were calculated from the TEM images (see inset in Fig. 2) yielding 12.9 and 18.9 nm for C-ZnO and O-ZnO, respectively. Differences observed in the degree of agglomeration, average particle size, and vacancy concentration are attributed to the different precipitating agents used.

Positron annihilation lifetime measurements (PALS) were also carried on to evaluate the defect structure of

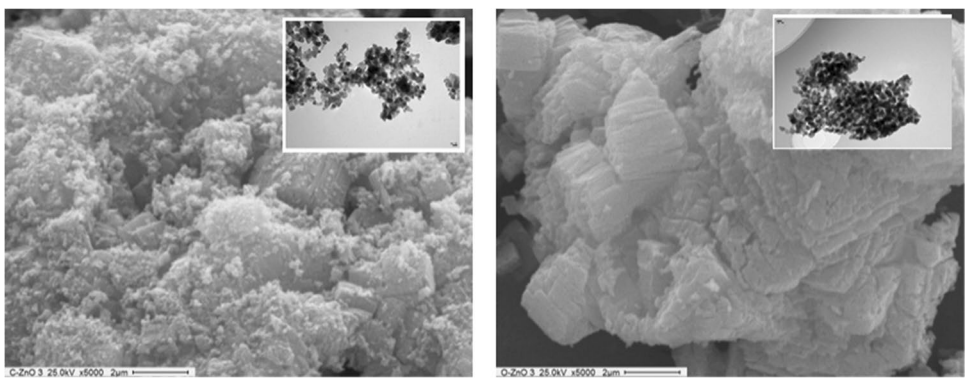

Fig. 2 SEM images 5000X **a** C-ZnO and **b** O-ZnO. The inset shows TEM images of both samples

the nanopowders. Experimental and analysis details can be found elsewhere [27]. Positron lifetime spectra were decomposed into three exponential decays, each one characterized by a positron lifetime τ_i of intensity I_i (see Fig. 3). The third lifetime is related to ortho positronium annihilation and has a very low relative intensity, so the lifetimes of interest here are the first two components. The longer the positron lifetime, the larger the defect size, so as it was previously discussed, τ_1 being higher than ZnO bulk lifetime (158 ps) is sensing, in addition, monovacancies. On the other side, the second lifetime τ_2 is sensing positrons trapped at larger size defects such as vacancy clusters (nanovoids) or at intersection interfaces (i.e., triple lines). In consequence, the ratio (I_1/I_2) between the relative intensity of these two events provides information on the relative concentration of defects. It is well known that ZnO presents vacancies in both sublattices, oxygen, and zinc, and as positron traps their lifetime was found experimentally to be 180 ps and 230 ps, respectively. Then, it may be concluded from PALS results that C-ZnO has more monovacancies and fewer high-size defects (divacancies or agglomeration of vacancies) than O-ZnO. These properties could be related to the antimicrobial efficiency exhibited by C-ZnO since they would favor the production of ROS, in the presence and absence of light, and the release of Zn^{2+} ions [50]. As noted above, both ROS and Zn^{2+} ions have been indicated as responsible for part of the mechanism of antimicrobial activity of these oxides [53].

Additionally, it has been reported an improvement in the antimicrobial activity of ZnO with a decrease in the bandgap [54, 55]. The decrease in the band gap of the samples (3.05 for O-ZnO and 2.99 for C-ZnO) is associated with the presence of energy levels within the band gap of the semiconductor, due to vacancy defects. Finally, the decrease in particle size is also a fundamental factor in antimicrobial activity, as mentioned above.

The determined parameters (particle size, energy gap, and vacancy concentration) by means of three experimental techniques (TEM, UV–vis, and positron lifetime spectroscopy) are displayed in Fig. 4. As it was previously discussed, the behavior observed in all of them is consistent with an increase in antimicrobial activity.

Therefore, it was achieved that the antimicrobial activity of C-ZnO is higher than that of O-ZnO. The most active material was the one with the smallest particle size and the highest concentration of VO^{++}. These facts lead to a better particle-fungus/bacteria interaction, as well as a higher availability of Zn^{2+} because of an incremental vacancy amount.

As mentioned above, the synthesis route leads to the formation of particles with differences in their properties, clearly indicating that the variation in the precipitating agent used plays a fundamental role.

Our results are in agree with many research papers that associate smaller particle sizes with higher antibacterial and antifungal activity. Soren et al. tested ZnO NPs of different crystalline sizes (10 and 20 nm) against bacteria and found increased toxicity by decreasing the size of the ZnO NPs [56]. Kalia et al. showed that the size of Zn NPs and their crystal chemistry can affect the fungicidal potential as these characteristics alter the ability to trespass the fungal cell wall and membrane structures

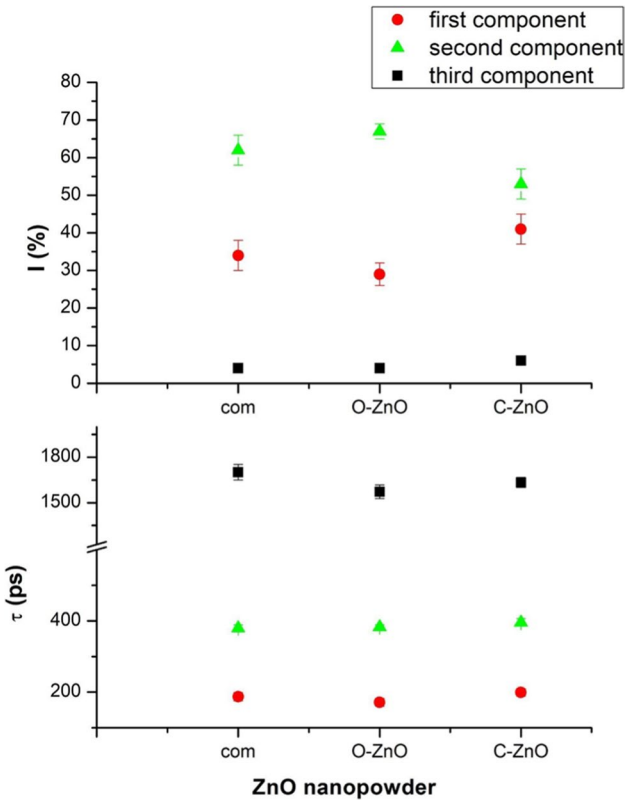

Fig. 3 Positron lifetime parameters for the studied samples: commercial powders (com), O-ZnO and C-ZnO

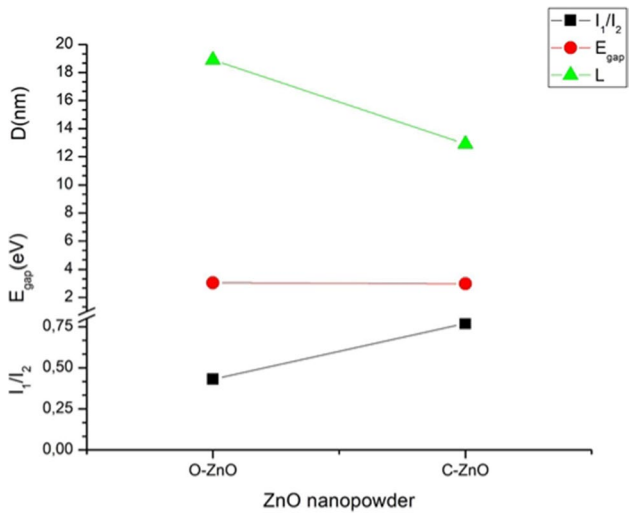

Fig. 4 Particle size (D), energy band gap (E_{gap}), and positron annihilation intensities ratio ($I/_1I_2$) for O-ZnO and C-ZnO

to elicit ROS response besides varying the dissolution of the ZnNPs within the cytoplasm [50]. Zakharova et al. found that smaller ZnO NP displayed higher toxicity than larger particles even in the presence of particle aggregation [57]. These authors also stated that it does not necessarily ZnO penetrate into the bacterial cells but its presence on the microenvironment around the bacteria is sufficient for killing them. Presumably, individual ZnO particles retain sufficient surface activity after aggregation.

Considering these results, C-ZnO was selected to perform the macrodilution test. The percentages of inhibition (% *I*) obtained in each case are presented in Table 2. At lower concentrations (1, 2, and 3 mg/mL) the growth of *C. globosum* was similar to that of the control during the 7 days of the test (% $I=0$). Plates with concentrations of 5, 10, and 15 mg/mL showed a different behavior from those mentioned before, as it can be seen in Table 2 and Fig. 5. In the Petri dishes with 5 mg/mL, a slow growth was observed while with 10 mg/mL it was reduced even more. Finally, the plates with 15 mg/mL did not show any growth after 7 days. Therefore, this concentration results in the minimum inhibitory concentration (MIC) for this strain, at least within the concentration range tested.

In the case of *A. fumigatus*, the inhibition percent for concentrations lower than 5 mg/mL showed similar results to *C. globosum*. The growth of *A. fumigatus* was reduced considerably in concentrations of 10 and 15 mg/mL and no growth was observed after 7 days as can be seen in Fig. 2. *A. fumigatus* showed to be more sensitive compared to *C. globosum* since its growth was more inhibited with lower concentrations. In this sense, the MIC (10 mg/mL) was lower than that obtained against *C. globosum* (15 mg/mL). It should be noted that in both cases a directly proportional relationship was observed between the concentration and the degree of inhibition, the higher the concentration of C-ZnO, the higher the inhibition.

3.2 Formulation, preparation, and characterization of the functional paints

According to the results shown in the previous section, C-ZnO was selected to elaborate a functional paint. Firstly,

Table 2 Inhibition percent (% *I*) of the fungal growth in solid medium with C-ZnO after 7 days

	C. globosum						
Concentration (mg/mL)	0	1	2	3	5	10	15
% *I*	0	0	0	0	43	86	100
	A. fumigatus						
Concentration (mg/mL)	0	1	2	3	5	10	15
% *I*	0	0	0	32	82	100	100

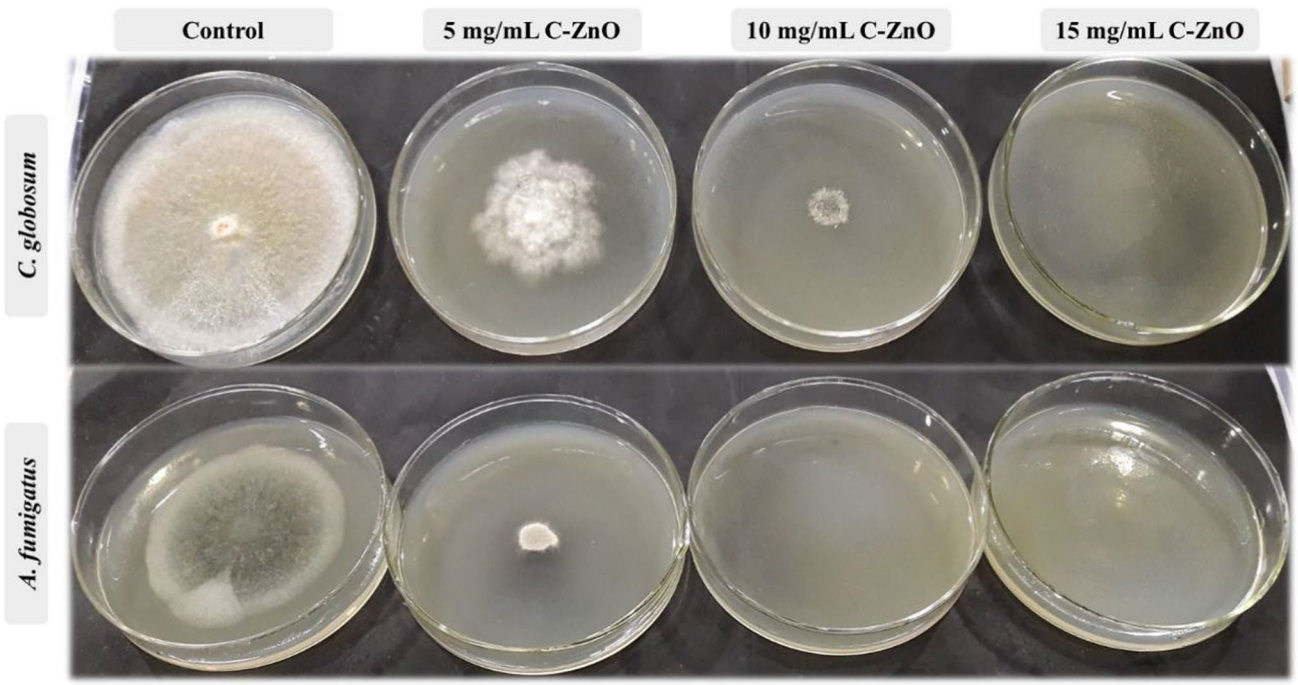

Fig. 5 Macrodilution assay: plates with and without C-ZnO after 7 days of incubation

control paint without biocides (CP) and paint with 1.5 g of C-ZnO per 100 g of total paint, labeled as 1.5% C-ZnO, were prepared. Regarding the relation to the concentration of ZnO NP in acrylic paints: it has been reported that acrylic coatings increase the absorption of UV-light by increasing the concentration of the ZnO NP which seems to be accentuated for concentrations ≥ 2 wt% [58]. In this sense, an excess in the concentration of ZnO NP (smaller in size than 30 nm) has been associated with resin (paint film-forming material) degradation [59]. This is consistent with literature indicating the advantages of using concentrations below 2 wt% which would be counteracting the photodegradation effect of the ZnO NP [60].

The results of the prepared paints characterization are listed in Table 3.

The color change (ΔE) and gloss were determined by measuring the CIElab color parameters (L, a, and b). The ΔE of the paint due to the addition of C-ZnO was 0.4. This ΔE is related to a slight change in visual appearance, concluding that the addition of C-ZnO did not produce significant changes in color in relation to the CP. This makes the use of ZnO NPs advantageous compared to Ag NP which causes an important color change of coatings due to the presence of pinkish Ag^+ ions [61]. Regarding gloss, no changes are observed between both paints being their values within the IRAM 1070 standard for interior paints.

The water absorption exhibited by the 1.5% C-ZnO sample was higher than that obtained from the CP while the permeability was lower. The permeabilities after the first 24 h were 0.19 and 0.15 g/cm^2 for CP and 1.5% C-ZnO, respectively, a trend that was maintained at 48 and 72 h. The differences in absorption and permeability could be due to the smaller C-ZnO particles being distributed among the micrometer-sized pigments (TiO_2 and $CaCO_3$), generating a different conformation in the film compared to the CP. This new arrangement in the coating would increase the surface area of the solids within the film. At this point, it is important to remember that there are volatile components in the formulation that are eliminated during the drying process and the non-volatile are those that form the solid protective film being responsible for its final properties [37]. In this sense, the size and shape of the particles affect the spatial distribution and the exposed surface of the components, which impact the film properties.

Two specific properties of liquid paint, such as viscosity and specific weight, did not show differences between one formulation and another, as given in Table 3. It should be noted that these values together with the degree of dispersion presented by the control paint are within the ranges required by the IRAM 1070 standard. Regarding the degree of dispersion, 1.5% C-ZnO sample shows a lower value compared to CP, which may be related to a certain degree of particle agglomeration present in the system.

3.3 Fungal resistance assay

CP and 1.5% C-ZnO paints were tested for their antifungal efficiency. The films were exposed to fungal growth for 4 weeks and afterward rated (R) using ASTM D5590 standard scale.

Figure 6 shows the results obtained with films inoculated with *C. globosum*. From the images obtained by stereomicroscope (Fig. 6a) an appreciable growth on control samples (CP) is observed yielding a value of R = 3, which is referred to as moderate. Instead, for the 1.5%, C-ZnO sample traces of growth are registered with R = 1, showing an important difference compared to the control.

SEM images (Fig. 6b) corroborate the results obtained by stereomicroscope. The spoilage imparted by *C. globosum* on CP samples is appreciated through an active growth with abundant mycelium and spores. In contrast, an ungerminated spore deposited on the surface at the time of inoculation on the 1.5% C-ZnO sample is seen (pointed out with a yellow circle in the micrograph, Fig. 6b).

Paints inoculated with *A. fumigatus* are shown in Fig. 6. The CP samples showed abundant growth (R = 4). On the other hand, the samples corresponding to 1.5% of C-ZnO were able to inhibit the growth (lower than light, R = 1–2) of the corresponding strain mostly observable on the edges. SEM micrographs corroborate the above observations (Fig. 6b), in particular, CP sample inoculated with *A. fumigatus* exhibits abundant reproductive structures (conidiophores) characteristic of this fungus, responsible for the release of many conidia. The degree of development in the paints with C-ZnO was lower, which was reflected in poor growth and inhibition of vegetative mycelium.

Table 3 Physical properties of the control and the 1.5% C-ZnO paints

Samples	Water adsorption (w/t %)	Color change(ΔE)	Viscosity (U.K.)	Dispersion (μm)	Specific weight (g/cm^3)	Hiding power (μm)
Control paint	10.8	–	98	50–60	1.4	225
1.5% C-ZnO	14.0	0.4	97	70–80	1.4	225

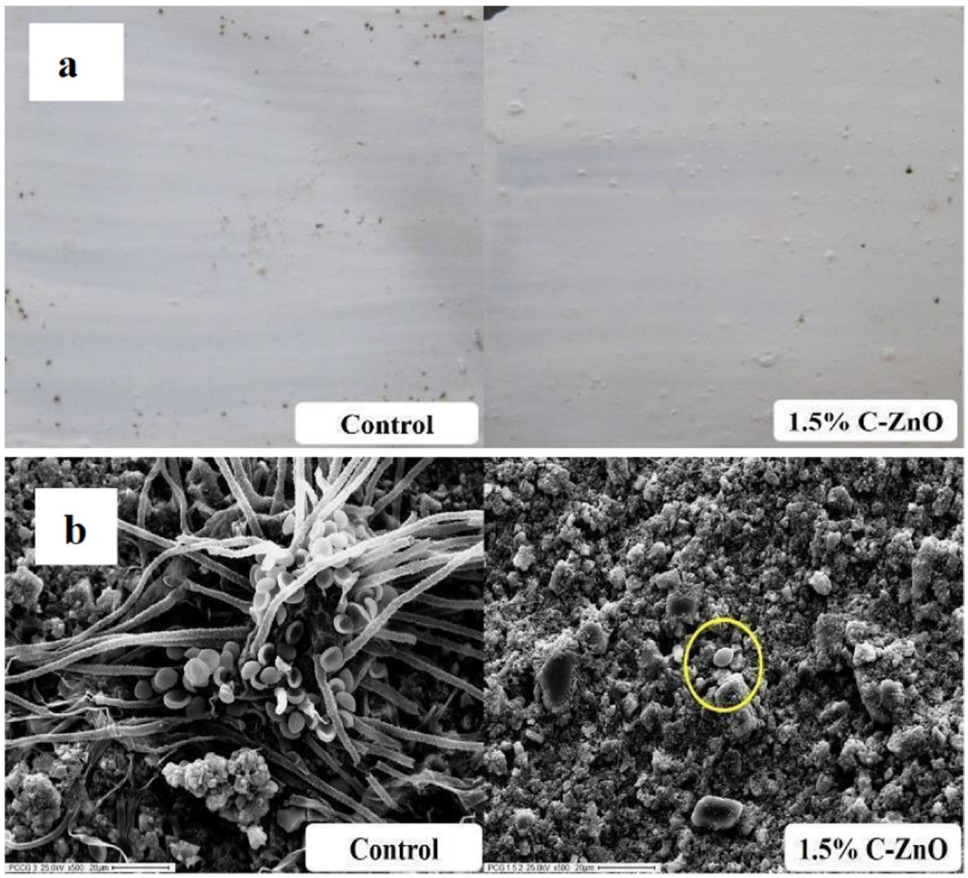

Fig. 6 Fungal resistance assay **a** photographs records and **b** SEM micrographs of the paints with and without C-ZnO after 4 weeks with *A. fumigatus*

Therefore, the paint with C-ZnO was probed to inhibit the growth of both fungal strains, *C. globosum*, and *A. fumigatus,* which shows that the C-ZnO particles managed to impart their antifungal activity in the paint film.

3.4 Bacterial biofilm resistance assay

The bacterial biofilm resistance of the paint films (CP and 1.5% C-ZnO) was evaluated in a liquid medium inoculated with *S. aureus*. SEM micrographs of coatings are shown in Fig. 7. *S. aureus* is widely used for this type of test due to its high capacity for biofilm formation. A constituted and widely distributed biofilm was exhibited by control samples from CP films. An active and abundant growth of *S. aureus* was observed, where the cellular morphology in the form of cocci characteristic of this strain can be seen (×2000 magnification). Adherent bacterial cells were not observed in films with

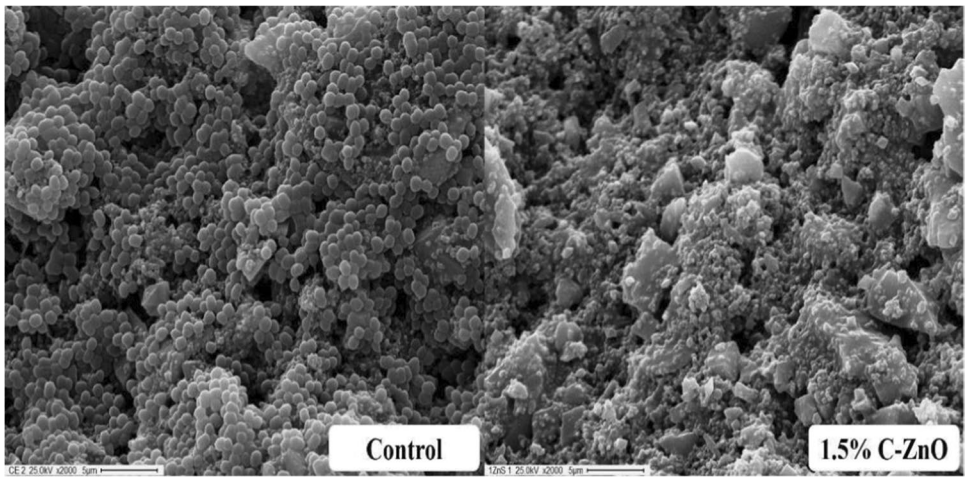

Fig. 7 SEM micrographs of paint films from bacterial biofilm resistance assay against *S. aureus*

1.5% C-ZnO, and therefore the conformation of biofilm was not found.

Following a similar trend to that observed in the preliminary agar diffusion tests, a greater sensitivity was also found in relation to the bacterial strain in the bio-resistance tests of the films.

4 Conclusions

Zinc oxides obtained from spent alkaline batteries showed promising antimicrobial activity against several pathogens. Both prepared oxides, C-ZnO and O-ZnO, inhibit the growth of *S. aureus* bacteria and *A. fumigatus* fungi, whereas *C. globosum* fungi is only inhibited by C-ZnO. The better performance of the last oxide can be explained by differences in the structural properties between the two compounds. The lower crystallite size and greater amount of oxygen monovacancies in C-ZnO would favor the availability of Zn^{2+} ions for their interaction with microbial cells. The 1.5% addition of the biocide does not significantly modify the physical properties of the paint and confers bioactive properties via the growth inhibition of the inoculated microorganisms.

Thus, it is possible to prepare functional paints with an antimicrobial activity using oxide metals from spent alkaline batteries as raw material. This research contributes to the comprehension of nanoparticles' effect on fungi and bacteria populating in buildings, a fundamental move from an environmental point of view.

On the other hand, the present study is framed within the principles of green chemistry, since it introduces a valorization of environmentally hazardous waste. We consider a novel way to help improve both human health and the environment through water-based paints.

Acknowledgements Our work was supported by grants from CONICET (Argentina Nacional Research Council); Comisión de Investigaciones Científicas de la Provincia de Buenos Aires (CICPBA)**;** Universidad Nacional de La Plata (UNLP) and by ANPCyT. Particular thanks to the service sector CIDEPINT (Ing. Mateo Paez and Diego Tunessi) and the technical support of Ing. Pablo Bellotti and Lic. Leyanet Barberia Roque.

Author contribution Guillermo Lopez: material preparation, data collection, and analysis. María V. Gallegos: conceptualization, material preparation, data collection and analysis, writing—original draft, writing—review and editing. Andres Peluso: writing—original draft, writing—review and editing. Laura Damonte: writing—original draft, writing—review and editing. Jorge Sambeth: supervision, writing—review and editing. Jorge Marchetti: funding acquisition, software, supervision, writing—review and editing. Natlia Belloti: material preparation, data collection, and analysis, writing—original draft, writing—review and editing. All authors read and approved the final manuscript.

Funding Our work was supported by grants from CONICET (Argentina National Research Council PIP 943); Facultad de Ciencias Exactas (UNLP, 11/X772, and 11/X X891) and by ANPCyT (Pict 2020 3529).

Declarations

Competing interests The authors declare no competing interests.

References

1. E.Y. Shaba, J.O. Jacob, J.O. Tijani, M.A.T. Suleiman, A critical review of synthesis parameters affecting the properties of zinc oxide nanoparticle and its application in wastewater treatment. Appl. Water. Sci. **11**, 48 (2021). https://doi.org/10.1007/s13201-021-01370-z
2. S. Faisal, H. Jan, S.A. Shah, S. Shah, A. Khan, M.T. Akbar, M. Rizwan, F. Jan, A. Wajidullah, A. Khattak, S. Syed, Green synthesis of zinc oxide (ZnO) nanoparticles using aqueous fruit extracts of myristica fragrans their characterizations and biological and environmental applications. ACS Omega **6**(14), 9709–9722 (2021). https://doi.org/10.1021/acsomega.1c00310
3. A. Rahman, M.H. Harunsani, A.L. Tan, M.M. Khan, Zinc oxide and zinc oxide-based nanostructures: biogenic and phytogenic synthesis, properties and applications. Bioprocess Biosyst. Eng. **44**(7), 1333–1372 (2021). https://doi.org/10.1007/s00449-021-02530-w
4. N. Tamimi, A. Mohammadi Nafchi, H. Hashemi-Moghaddam, H. Baghaie, The effects of nano-zinc oxide morphology on functional and antibacterial properties of tapioca starch bionanocomposite. Food Sci. Nutr. **9**(8), 4497–4508 (2021). https://doi.org/10.1002/fsn3.2426
5. X. Li, L. Zhang, Z. Wang, S. Wu, J. Ma, Cellulose controlled zinc oxide nanoparticles with adjustable morphology and their photocatalytic performances. Carbohyd. Polym. **259**, 117752 (2021). https://doi.org/10.1016/j.carbpol.2021.117752
6. A. Pinkas, N. Waiskopf, S. Gigi, T. Naor, A. Layani, U. Banin, Morphology effect on zinc oxide quantum photoinitiators for radical polymerization. Nanoscale **13**(15), 7152–7160 (2021). https://doi.org/10.1039/d1nr00896j
7. A.K. Bhunia, S. Saha, Characterization of zinc oxide nanocrystals with different morphology for application in ultraviolet-light photocatalytic performances on rhodamine B. Luminescence **36**(1), 149–162 (2020). https://doi.org/10.1002/bio.3930
8. K.G. Akpomie, S. Ghosh, M. Gryzenhout, M, J. Conradie, One-pot synthesis of zinc oxide nanoparticles via chemical precipitation for bromophenol blue adsorption and the antifungal activity against filamentous fungi. Sci. Rep. **11**(1) (2021). https://doi.org/10.1038/s41598-021-87819-2
9. M.S. Saif, A. Zafar, M. Waqas, S.G. Hassan, A. Haqul, T. Tariq, S. Batool, M. Dilshad, M. Hasan, X. Shu, Phyto-reflexive zinc oxide nano-flowers synthesis: an advanced photocatalytic degradation and infectious therapy. J. Market. Res. **13**, 2375–2391 (2021). https://doi.org/10.1016/j.jmrt.2021.05.107
10. S.M.E. Sepasgozar, S. Mohseni, B. Feizyzadeh, A. Morsali. Green synthesis of zinc oxide and copper oxide nanoparticles using Achillea Nobilis extract and evaluating their antioxidant and antibacterial properties. Bull. Mater. Sci. **44**(2) (2021). https://doi.org/10.1007/s12034-021-02419-0
11. A. Sirelkhatim, S. Mahmud, A. Seeni, N.H.M. Kaus, L.C. Ann, S.K.M. Bakhori, H. Hasan, D. Mohamad, Review on zinc oxide nanoparticles: Antibacterial activity and toxicity mechanism. Nano-Micro Letters **7**(3), 219–242 (2015). https://doi.org/10.1007/s40820-015-0040-x
12. E.O. Ogunsona, R. Muthuraj, E. Ojogbo, O. Valerio, T.H. Mekonnen, Engineered nanomaterials for antimicrobial applications: a review. Appl. Mater. Today. **18**, 100473 (2020). https://doi.org/10.1016/j.apmt.2019.100473

13. A. Nigam, S. Saini, A.K. Rai, S.J. Pawar, Structural, optical, cytotoxicity, and antimicrobial properties of MgO, ZnO and MgO/ZnO nanocomposite for biomedical applications. Ceram. Int. **47**, 19515–19525 (2021). https://doi.org/10.1016/j.ceramint.2021.03.289
14. Y. Liu, C. Xu, Z. Zhu, J. Lu, A.G. Manohari, Z. Shi, Self-assembled ZnO/Ag hollow spheres for effective photocatalysis and bacteriostasis. Mater. Res. Bull. **98**, 64–69 (2018). https://doi.org/10.1016/j.materresbull.2017.09.057
15. L. Zhang, Y. Ding, M. Povey, D. York, ZnO nanofluids-A potential antibacterial agent. Prog. Nat. Sci. **18**, 939–944 (2008). https://doi.org/10.1016/j.pnsc.2008.01.026
16. S. Umavathi, S. Mahboob, M. Govindarajan, K.A. Al-Ghanim, Z. Ahmed, P. Virik, N. Al-Mulhm, M. Subash, K. Gopinath, C. Kavitha, Green synthesis of ZnO nanoparticles for antimicrobial and vegetative growth applications: a novel approach for advancing efficient high quality health care to human wellbeing, Saudi. J. Biol. Sci. **28**, 1808–1815 (2021). https://doi.org/10.1016/j.sjbs.2020.12.025
17. T. Reddy, Linden's Handbook of Batteries, 4th ed., New York, 2011
18. E.M. Melchor-Martínez, R. Macias-Garbett, A. Malacara-Becerra, H.M.N. Iqbal, J.E. Sosa-Hernández, R. Parra-Saldívar, Environmental impact of emerging contaminants from battery waste: a mini review. Case Stud. Chem. Environ. Eng. **3**, 100104 (2021). https://doi.org/10.1016/j.cscee.2021.100104
19. M. Täubel, A. Hyvärinen, Occurrence of mycotoxins in indoor environments. Elsevier (2015). https://doi.org/10.1016/B978-0-12-411471-5.00018-1
20. J. Hurraß, B. Heinzow, U. Aurbach, K.C. Bergmann, A. Bufe, W. Buzina, O.A. Cornely, S. Engelhart, G. Fischer, T. Gabrio, W. Heinz, C.E.W. Herr, J. Kleine-Tebbe, L. Klimek, M. Köberle, H. Lichtnecker, T. Lob-Corzilius, R. Merget, N. Mülleneisen, D. Nowak, U. Rabe, M. Raulf, H.P. Seidl, J.O. Steiß, R. Szewszyk, P. Thomas, K. Valtanen, G.A. Wiesmüller, Medical diagnostics for indoor mold exposure. Int. J. Hyg. Environ. Health. **220**, 305–328 (2017). https://doi.org/10.1016/j.ijheh.2016.11.012
21. T. Verdier, M. Coutand, A. Bertron, C. Roques, A review of indoor microbial growth across building materials and sampling and analysis methods. Build. Environ. **80**, 136–149 (2014). https://doi.org/10.1016/j.buildenv.2014.05.030
22. S.Y. Lee, S.H. Kim, C.Y. Hong, M.J. Park, I.G. Choi, Effects of (-)-borneol on the growth and morphology of Aspergillus fumigatus and Epidermophyton floccosom, Flavour. Fragr. J. **28**, 129–134 (2013). https://doi.org/10.1002/ffj.3138
23. D.J. Weber, H. Kanamori, W.A. Rutala, "No touch" technologies for environmental decontamination: focus on ultraviolet devices and hydrogen peroxide systems. Curr. Opin. Infect. Dis. **29**, 424–431 (2016). https://doi.org/10.1097/QCO.0000000000000284
24. A. Afshari, H.R. Anderson, A. Cohen, Ed. de Oliveira Fernandes, J. Douwes, R. Górn, Maija-Riitta Hirvonen, J. Jaakkola, S. Kirchner, J. Kurnitski, H. Levin, M. Mendell, L. Mølhave, L. Morawska, A. Nevalainen, M. Richardson, P. Rudnai, H. W. Schleibinger, Per E. Schwarze, B. Seifert, T. Sigsgaard, W. Song, J. Spengler, R. Szewzyk, S. Panchatcharam Thyagarajan, G. Gallo, M. Giersig, J. Hjort Bønløkke, K. Cheung, A. G. Mirer, H. W. Meyer, M. Roponen, WHO guidelines for indoor air quality: dampness and mould. In WHO guidelines for indoor air quality: dampness and mould World Health Organization (2009)
25. D.M.G.A. Tressmann, L.G. Pedroti, A.F. de Carvalho, J.C.L. Ribeiro, F. de Paula Cardoso, M.M.S. Lopes, A.F. de Oliveira, S.O. Ferreira. Research into the use of marble waste as mineral filler in soil pigment-based paints and as an active pigment in waterborne paints. Constr. Build. Mater. **241**, 117976 (2020). https://doi.org/10.1016/j.conbuildmat.2019.117976.
26. P. Ganguli, S. Chaudhuri, Nanomaterials in antimicrobial paints and coatings to prevent biodegradation of man-made surfaces: a review. Mater. Today Proc. **45**, 3769–3777 (2020). https://doi.org/10.1016/j.matpr.2021.01.275
27. M.V. Gallegos, F. Aparicio, M.A. Peluso, L.C. Damonte, J.E. Sambeth, Structural, optical and photocatalytic properties of zinc oxides obtained from spent alkaline batteries. Mater. Res. Bull. **103**, 158–165 (2018). https://doi.org/10.1016/j.materresbull.2018.03.022
28. M.V. Gallegos, L.R. Falco, M.A. Peluso, J.E. Sambeth, H.J. Thomas. Recovery of manganese oxides from spent alkaline and zinc–carbon batteries. An application as catalysts for VOCs elimination. Waste Manage. **33**(6), 1483–1490 (2013). https://doi.org/10.1016/j.wasman.2013.03.006
29. M.V. Gallegos, M.A. Peluso, J.E. Sambeth, Preparation and characterization of manganese and zinc oxides recovered from spent alkaline and zn/c batteries using biogenerated sulfuric acid as leaching agent. JOM **70**(10), 2351–2358 (2018). https://doi.org/10.1007/s11837-018-3043-5
30. N. Bellotti, R. Romagnoli, C. Quintero, C. Domínguez-Wong, F. Ruiz, C. Deyá, Nanoparticles as antifungal additives for indoor water borne paints. Prog. Org. Coatings. **86**, 33–40 (2015). https://doi.org/10.1016/j.porgcoat.2015.03.006
31. S. Roselli, C. Deyá, N. Bellotti. Fungal deteriorationof anti-corrosive coatings. Fungal deterioration of anti-corrosive coatings. Paint & Coating Industry http://sedici.unlp.edu.ar/handle/10915/120473
32. M.A. Fernández, L. Barberia Roque, E. Gámez Espinosa, C. Deyá, N. Bellotti. Organo-montmorillonite with biogenic compounds to be applied in antifungal coatings. Appl. Clay Sci. **184**, 105369 (2020). https://doi.org/10.1016/j.clay.2019.105369.
33. J. Magnusson, J. Schnürer. Lactobacillus coryniformis subsp. coryniformis strain Si3 produces a broad-spectrum proteinaceous antifungal compound. Appl. Environ. Microbiol. **67**, 1–5 (2001). https://doi.org/10.1128/AEM.67.1.1-5.2001.
34. N. Bellotti, L. Salvatore, C. Deyá, M.T. Del Panno, B. del Amo, R. Romagnoli, The application of bioactive compounds from the food industry to control mold growth in indoor waterborne coatings. Colloids Surfaces B Biointerfaces. **104**, 140–144 (2013). https://doi.org/10.1016/j.colsurfb.2012.11.037
35. L. Barberia-Roque, O.F. Obidi, E. Gámez-Espinosa, M. Viera, N. Bellotti, Hygienic coatings with bioactive nano-additives from Senna occidentalis-mediated green synthesis. NanoImpact. **16**, 100184 (2019). https://doi.org/10.1016/j.impact.2019.100184
36. L. Barberia-Roque, E. Gámez-Espinosa, M. Viera, N. Bellotti, Assessment of three plant extracts to obtain silver nanoparticles as alternative additives to control biodeterioration of coatings. Int. Biodeterior. Biodegrad. **141**, 52–61 (2019). https://doi.org/10.1016/j.ibiod.2018.06.011
37. V. Lakshmi Prasanna, R. Vijayaraghavan, Insight into the mechanism of antibacterial activity of zno: Surface defects mediated reactive oxygen species even in the dark. Langmuir **31**(33), 9155–9162 (2015). https://doi.org/10.1021/acs.langmuir.5b02266
38. C.R. Mendes, G. Dilarri, C.F. Forsan, V. de M. R. Sapata., P.R.M. de Lopes, P.B Moraes, R.N. Montagnolli, H. Ferreira, E.D. Bidoia, Antibacterial action and target mechanisms of zinc oxide nanoparticles against bacterial pathogens. Sci. Rep. **12**(1) (2022). https://doi.org/10.1038/s41598-022-06657-y
39. N. A. R. Gow, J.-P. Latge, & C. A. Munro. The fungal cell wall: Structure, biosynthesis, and function. Microbiology Spectrum, **5**(3) (2017). https://doi.org/10.1128/microbiolspec.funk-0035-2016
40. I.S. Okeke, K.K. Agwu, A.A. Ubachukwu, F.I. Ezema, Influence of transition metal doping on physiochemical and antibacterial properties of ZnO Nanoparticles: a review. Applied Surface

Science Advances **8**, 100227 (2022). https://doi.org/10.1016/j.apsadv.2022.100227
41. J.A. Romaniuk, L. Cegelski. Bacterial cell wall composition and the influence of antibiotics by cell-wall and whole-cell NMR. Philos. Trans. R. Soc. Lond., B, Biol. Sci. **370**, 20150024 (2015). https://doi.org/10.1098/rstb.2015.0024
42. O. Zakharova, E. Kolesniov, E. Vishnyakova, N. Strekalova, A. Gusev, Antibacterial activity of ZnO nanoparticles: dependence on particle size, dispersion media and storage time IOP. Conf. Ser. Earth Environ. Sci. **226**, 012062 (2019). https://doi.org/10.1088/1755-1315/226/1/012062
43. B. Lallo da Silva, B.L. Caetano, B.G. Chiari-Andreo, R.C.L.R Pietro, L.A. Chiavacci. Increased antibacterial activity of ZnO nanoparticles: influence of size and surface modification. Colloids Surf. B Bioi **177**, 440–447 (2019). https://doi.org/10.1016/j.colsurfb.2019.02.013
44. V.L. Prasanna, R. Vijayaraghavan, Insight into the mechanism of antibacterial activity of ZnO: surface defects mediated reactive oxygen species even in the dark. Langmuir **31**, 9155–9162 (2015). https://doi.org/10.1021/acs.langmuir.5b02266
45. B. Abebe, E.A. Zereffa, A. Tadesse, H.C.A. Murthy. A review on enhancing the antibacterial activity of zno: mechanisms and microscopic investigation. Nanoscale Research Letters. **15**(1) (2020). https://doi.org/10.1186/s11671-020-03418-6
46. H. Agarwal, S. Menon, S. Venkat Kumar, S. Rajeshkumar, Mechanistic study on antibacterial action of zinc oxide nanoparticles synthesized using green route. Chem. Biol. Interact. **286**, 60–70 (2018). https://doi.org/10.1016/j.cbi.2018.03.008
47. C.R. Mendes, G. Dilarri, C.F. Forsan, M.R.V. de Sapata, P.R.M., de Lopes, P.B. Moraes, R.N. Montagnolli, H. Ferreira, E.D. Bidoia. Antibacterial action and target mechanisms of zinc oxide nanoparticles against bacterial pathogens. Scientific Reports. **12**(1) (2022b). https://doi.org/10.1038/s41598-022-06657-y
48. V.J. Raj, R. Ghosh, A. Girigoswami, K. Girigoswami, Application of zinc oxide nanoflowers in environmental and biomedical science. BBA Advances **2**, 100051 (2022). https://doi.org/10.1016/j.bbadva.2022.100051
49. L.P. Mosquera-Sánchez, P.A. Arciniegas-Grijalba, M.C. Patiño-Portela, B.E. Guerra–Sierra, J.E. Muñoz-Florez, J.E. Rodríguez-Páez. Antifungal effect of zinc oxide nanoparticles (ZnO-NPs) on Colletotrichum sp., causal agent of anthracnose in coffee crops. Biocatal. Agric. Biotechnol. **25**, 101579 (2020). https://doi.org/10.1016/j.bcab.2020.101579
50. A. Kalia, J. Kaur, M. Tondey, P. Manchanda, P. Bindra, M.A. Alghuthaymi, A. Shami, K.A. Abd-Elsalam, Differential antimycotic and antioxidant potentials of chemically synthesized zinc-based nanoparticles derived from different reducing/complexing agents against pathogenic fungi of maize crop. J. Fungi **7**(3), 223 (2021). https://doi.org/10.3390/jof7030223
51 B.H. Shnawa, S.M. Hamad, A.A. Barzinjy, P.A. Kareem, M.H. Ahmed, Scolicidal activity of biosynthesized zinc oxide nanoparticles by Mentha longifolia L leaves against Echinococcus granulosus protoscolices. Emergent. Materials. **5**(3), 683–693 (2021). https://doi.org/10.1007/s42247-021-00264-9
52. D.J. da Silva, A. Duran, A.D. Cabral, F.L.A. Fonseca, R.F. Bueno, D.S. Rosa, Questioning ZnO, Ag, and Ag/ZnO nanoparticles as antimicrobial agents for textiles: do they guarantee total protection against bacteria and SARS-CoV-2? J. Photochem. Photobiol., B **234**, 112538 (2022). https://doi.org/10.1016/j.jphotobiol.2022.112538
53. X. Zhu, J. Wang, L. Cai, Y. Wu, M. Ji, H. Jiang, J. Chen, Dissection of the antibacterial mechanism of zinc oxide nanoparticles with manipulable nanoscale morphologies. J. Hazard. Mater. **430**, 128436 (2022). https://doi.org/10.1016/j.jhazmat.2022.128436
54. D.E. Navarro-López, R. Garcia-Varela, O. Ceballos-Sanchez, A. Sanchez-Martinez, G. Sanchez-Ante, K. Corona-Romero, D.A. Buentello-Montoya, A. Elías-Zuñiga, E.R. López-Mena. Effective antimicrobial activity of ZnO and Yb-doped ZnO nanoparticles against Staphylococcus aureus and Escherichia coli, Mater. Sci. Eng. C. **123** (2021). https://doi.org/10.1016/j.msec.2021.112004
55. G.N. Rajivgandhi, G. Ramachandran, N.S. Alharbi, S. Kadaikunnan, J.M. Khaleed, N. Manokaran, W.J. Li. Substantial effect of Cr doping on the antimicrobial activity of ZnO nanoparticles prepared by ultrasonication process. Mater. Sci. Eng. B Solid-State Mater. Adv. Technol. **263**, 114817 (2021). https://doi.org/10.1016/j.mseb.2020.114817
56. S. Soren, S. Kumar, S. Mishra, P.K. Jena, S. Verma, P. Parhi, Evaluation of antibacterial and antioxidant potential of the zinc oxide nanoparticles synthesized by aqueous and polyol method. Microb. Pathog. **119**, 145–151 (2018). https://doi.org/10.1016/j.micpath.2018.03.048
57. O. Zakharova, E. Kolesnikov, E. Vishnyakova, N. Strekalova, A. Gusev, Antibacterial activity of ZnO nanoparticles: dependence on particle size, dispersion media and storage time. IOP Conference Series: Earth and Environmental Science **226**, 012062 (2019). https://doi.org/10.1088/1755-1315/226/1/012062
58. T.V. Nguyen, P.H. Dao, K.L. Duong, Q.H. Duong, Q.T. Vu, A.H. Nguyen, V.P. Mac, T.L. Le, Effect of R-TiO 2 and ZnO nanoparticles on the UV-shielding efficiency of water-borne acrylic coating. Prog. Org. Coat. **110**, 114–121 (2017). https://doi.org/10.1016/j.porgcoat.2017.02.017
59. M. Eren, H.K. Can, Preparation of zinc methacrylate-methylmethacrylate-butyl acrylate emulsions and their application in exterior paints. Prog. Org. Coat. **135**, 424–437 (2019). https://doi.org/10.1016/j.porgcoat.2019.06.031
60. G.G. Goourey, P. Wong-Wah-Chung, L. Balan, Y. Israëli, Effects of ZnO quantum dots on the photostability of acrylate photopolymers used as recording materials. Polym. Degrad. Stab. **153**, 172–184 (2018). https://doi.org/10.1016/j.polymdegradstab.2018.04.026
61. M.C. Chen, P.W. Koh, V.K. Ponnusamy, S.L. Lee, Titanium dioxide and other nanomaterials based antimicrobial additives in functional paints and coatings: review. Prog. Org. Coat. **163**, 106660 (2022). https://doi.org/10.1016/j.porgcoat.2021.106660